Published online 16 March 2016

Nucleic Acids Research, 2016, Vol. 44, No. 9 ***4425–4439***
doi: 10.1093/nar/gkw184

Exclusion of small terminase mediated DNA threading models for genome packaging in bacteriophage T4

Song Gao[1,2], Liang Zhang[1] and Venigalla B. Rao[1,*]

[1]Department of Biology, The Catholic University of America, 620 Michigan Avenue Northeast, Washington, DC 20064, USA and [2]Jiangsu Key Laboratory of Marine Pharmaceutical Compound Screening, Huaihai Institute of Technology, Lianyungang 222005, China

Received February 09, 2016; Revised March 03, 2016; Accepted March 04, 2016

ABSTRACT

Tailed bacteriophages and herpes viruses use powerful molecular machines to package their genomes. The packaging machine consists of three components: portal, motor (large terminase; TerL) and regulator (small terminase; TerS). Portal, a dodecamer, and motor, a pentamer, form two concentric rings at the special five-fold vertex of the icosahedral capsid. Powered by ATPase, the motor ratchets DNA into the capsid through the portal channel. TerS is essential for packaging, particularly for genome recognition, but its mechanism is unknown and controversial. Structures of gear-shaped TerS rings inspired models that invoke DNA threading through the central channel. Here, we report that mutations of basic residues that line phage T4 TerS (gp16) channel do not disrupt DNA binding. Even deletion of the entire channel helix retained DNA binding and produced progeny phage *in vivo*. On the other hand, large oligomers of TerS (11-mers/12-mers), but not small oligomers (trimers to hexamers), bind DNA. These results suggest that TerS oligomerization creates a large outer surface, which, but not the interior of the channel, is critical for function, probably to wrap viral genome around the ring during packaging initiation. Hence, models involving TerS-mediated DNA threading may be excluded as an essential mechanism for viral genome packaging.

INTRODUCTION

Tailed bacteriophages are probably the most abundant forms of life on Earth (1). Genome packaging, a key step in the assembly of these viruses, thus, constitutes a significant portion of biological energy transactions occurring on the planet. These phages as well as their eukaryotic descendants such as herpes viruses employ powerful molecular machines to forcibly translocate DNA into a preformed empty capsid known as procapsid or prohead (2–6).

In the *myoviridae* phage T4, ∼171 kb, 56 μm-long genomic DNA is packaged into a 120 nm × 86 nm capsid to near crystalline density (7). The packaging machine consists of three essential components: i) TerS or the small 'terminase' (gp16), which recognizes the newly replicated viral genome, a head-tail concatemer that in T4 is extensively branched (8); ii) TerL or the large terminase (gp17), which forms a complex with TerS (holo-terminase) and makes a cut in the genomic DNA to initiate genome packaging (9,10); TerL also contains an ATPase activity that provides energy for DNA packaging (11–13); and iii) the dodecameric portal assembly (gp20), which is located at the special 5-fold vertex of the icosahedral capsid (14,15). It provides a channel through which DNA is transported into the capsid as well as a platform for assembly of gp17 into an oligomeric molecular motor. The phage T4 machine packaging at a rate of up to ∼2000 bp/sec is the fastest and most powerful machine reported to date (16).

The structures of all three packaging components have been determined from different viruses. They revealed highly conserved structural features even though there is no significant sequence similarity (6). For instance, the dodecameric portal is a cone-shaped structure consisting of crown and wing domains at the wider mouth located inside the capsid, stem domain that forms a channel, and clip domain that protrudes out at the vertex (15,17–20). TerL consists of two domains, an N-terminal ATPase domain and a C-terminal nuclease/translocase domain linked by a flexible hinge (21,22). The ATPase domain contains two subdomains; subdomain I having all the canonical signatures such as Walker A, Walker B, and catalytic carboxylate, and subdomain II having the regulatory sites. Cryo-EM structure of the prohead–gp17 complex showed a pentameric motor with five gp17 molecules assembled on the portal's clip domain (Figure 1A). An electrostatic force dependent DNA packaging mechanism was proposed in which the C-domain bound to DNA, powered by ATP hydrolysis by the N-domain, moves in a piston-like fashion translocating 2-bp of DNA at a time (22).

*To whom correspondence should be addressed. Tel: +1 202 319 5271; Fax: +1 202 319 5721; Email: rao@cua.edu

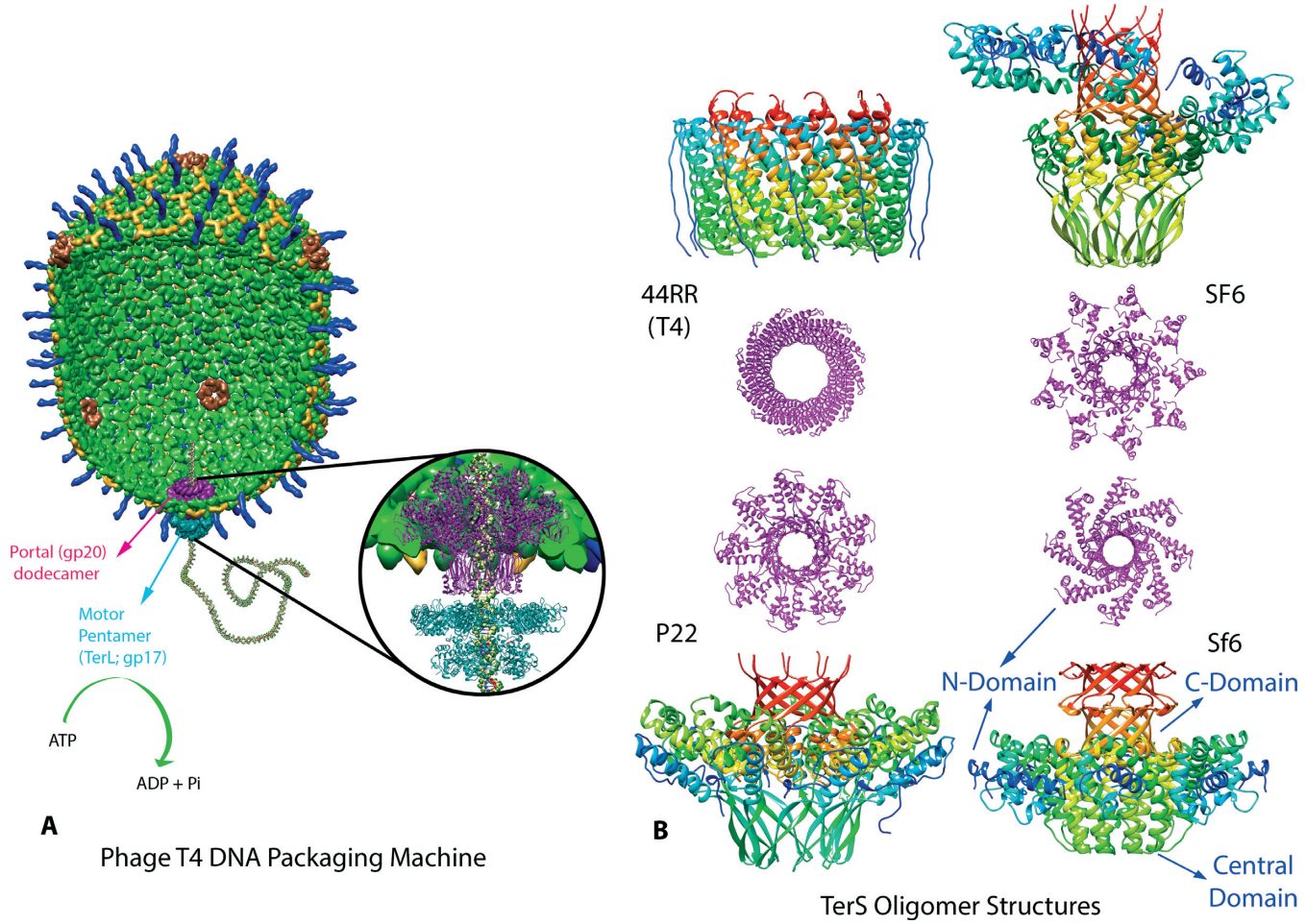

Figure 1. Components of the bacteriophage T4 DNA packaging machine. (**A**) Structural model of the minimal phage T4 DNA packaging machine. It consists of the pentameric motor assembled at the dodecameric portal vertex of the capsid (22). (**B**) X-ray structures of TerS oligomers from different phages (T4-related phage 44RR, PDB code: 3TXQ (25); P22, PDB code: 3P9A (23); Sf6, PDB code: 3HEF (24)). The SF6 structure is a model built using the X-ray structures of full-length TerS (trimer in the asymmetric unit containing two N-domains at different spatial positions; PDB code: 3ZQQ (26)) and truncated TerS lacking the N-terminal domains (amino acids 65–141; nanomer; PDB code: 3ZQP (26)). The structures are shown in rainbow colours ranging from blue at the N-terminus to red at the C-terminus. The top views of the structures are shown in the center (magenta). The subdomains are labeled in the Sf6 TerS structure.

TerS from different phages forms stable oligomers, gear-shaped rings with a central channel (23–26) (Figure 1B). The proteins fold similarly but the stoichiometry of the oligomers and the diameter of the channel vary (Figure 1B, top views shown in magenta). Phage Sf6 TerS forms octamers and nonamers (21,27), SF6 forms nonamers and decamers (26), SPP1 and P22 form nonamers (23,26), and T4 and the related phage 44RR form 11-mers and 12-mers (25,28). But they all contain three domains; an N-terminal globular domain, a central oligomerization domain, and a C-terminal β-barrel domain. The N-terminal domain is predicted to contain a helix-turn-helix motif (2,25,29) that in phages λ, SPP1, SF6 and Sf6 has been shown to bind DNA (26,30–32). The N-domains encircle the wider end of the vase-shaped core, often via a flexible linker connecting the N-and oligomerization domains. The C-terminal domain contains 1–3 β-strands that form a helical barrel which projects upwards from the centre of the vase (Figure 1B). Swapping this domain between related phages, such as T4 and RB49, leads to swapping of TerL specificity suggesting that this domain is involved in recruiting TerL (33–35).

One of the most intriguing aspects of viral DNA packaging is how TerS initiates DNA packaging at a single site (or very few sites) on the concatemeric genome. Most phage TerS proteins recognize a specific sequence such as *cos* (λ phages) or *pac* (P22, SPP1) that spans ∼150–200 bp and resides near or within the TerS coding sequence (31,34,36). The sequence specificity probably allows the virus to exclude the host genome from packaging into its capsid. However, phage T4 degrades the unmodified host DNA and hence, lacks strict sequence specificity. Notwithstanding these differences, a common feature of all TerSs is the formation of a higher order TerS-DNA complex which by interaction with TerL forms a ternary holo-terminase complex that cuts DNA and initiates packaging (2,3,36).

The structure of the TerS-DNA complex is unknown and controversial. Two different models have been proposed; DNA wrapping and DNA threading (Figure 2). In the wrapping model, the putative DNA binding N-domains

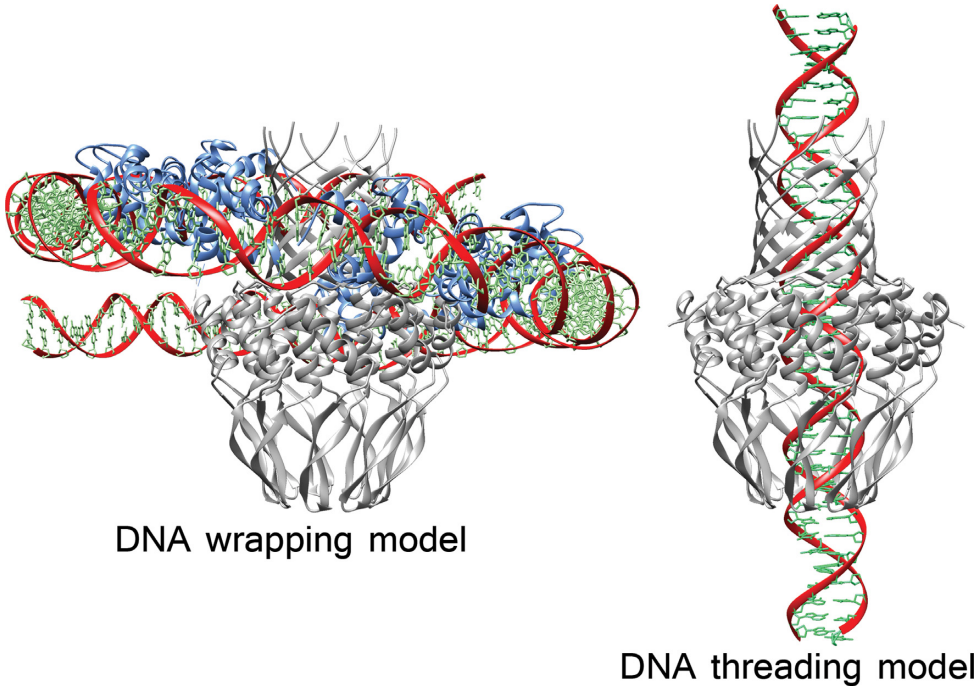

Figure 2. Models of TerS–DNA complex. In the wrapping model, DNA interacts with the N-domains that encircle the central core (26). In the threading model, DNA passes through the central channel. SF6 TerS was used for generating the models (wrapping model was kindly provided by Dr Fred Antson, University of York, UK). The central domains and C-domains are shown in gray and the N-domains (wrapping model) are shown in cyan (26). DNA clashes with the channel residues in the threading model (the N-domains are not shown in the threading model).

by virtue of their location around the perimeter of TerS oligomer wrap the DNA around the ring (24–26). The inter-domain linker is supposed to provide flexibility to bend the DNA in order to allow wrapping (26,32,34). In the threading model, DNA goes through the TerS channel with the residues lining the lumen interacting with the phosphate backbone (DNA threading is defined as the insertion and/or movement of DNA through a channel without reference to a specific packaging mechanism) (3,24,27,37,38) (Figure 2). However, wrapping and threading need not be mutually exclusive. Wrapping might assemble a nucleosome-like structure while threading might position the DNA for TerL cutting. Aligned with the TerL and portal channels, TerS can then activate TerL's packaging ATPase and help ratchet the cut end into the capsid.

Here, we investigated the central question underlying the DNA threading models: is the TerS channel essential for function? We first developed DNA binding assays that demonstrated that the WT T4 gp16 binds DNA, both *in vitro* and *in vivo*. We then mutated the basic residues that line the TerS channel which, contrary to the expectation, did not disrupt DNA binding. Remarkably, even the deletion of the entire channel helix retained DNA binding *in vitro* and produced phage *in vivo*. Further, we discovered that some of the mutants produced two types of oligomers; higher oligomers that are similar in size to the WT (11- and 12-mers) and lower oligomers that are in the range of trimers to hexamers. Irrespective of the mutant, higher oligomers bound DNA but the lower oligomers did not. These results lead to the conclusion that TerS oligomerization that creates a large outer surface of the ring, but not the interior of the channel, is essential for DNA packaging. Hence, models that invoke TerS mediated DNA threading for phage DNA packaging may be excluded as a common or essential mechanism.

MATERIALS AND METHODS

Bacteria, plasmids and phage

Escherichia coli XL10-Gold Ultra competent cells (Agilent Technologies, Santa Clara, CA, USA) were used for selecting and maintaining the T4 gp16 recombinant plasmids. *E. coli* BL21 (DE3) RIPL (*sup*$^-$) cells (Agilent Technologies) were used for overexpression of gp16 proteins, construction of T4 phage mutants, and for marker rescue experiments. *E. coli* P301 (*sup*$^-$) strain was used for amplification of gene 16 (*g16*) mutants. The expression vector pET-28b (Novagen-EMD Biosciences, Merck KGaA, Darmstadt, Germany) was used for construction of gp16 expression plasmids. The T4.16Q114am (gp16 Q114 amber) phage (39) was used for selection of T4 phage mutants by marker rescue. T4 phage DNA purified by the phenol–chloroform extraction procedure was used as a template for PCR amplification of *g16* DNA.

Cloning, expression, and purification of gp16 constructs

DNA fragments of *g16* were amplified by PCR using Phusion (New England Biolabs, Ipswich, MA) or KOD (NOVA, LCP Biomed Co., Lianyungang, China) DNA polymerase with appropriate primers. For point mutations or sequence deletions in the middle of *g16* gene, the PCR-directed splic-

ing by overlap extension strategy was used (40,41). Amplified DNA fragments were digested with appropriate restriction enzymes (Thermo Fisher Scientific, Inc., Waltham, MA, USA) and ligated into pET-28b vector, resulting in the fusion of a hexa-histidine tag to the N-terminus of each construct. Ligated DNAs were transformed into *E. coli* XL10-Gold Ultra competent cells for plasmid amplification. The plasmid DNAs were purified using the GeneJET plasmid miniprep kit (Thermo Fisher Scientific, Inc.). Accuracy of the cloned DNA was ascertained by DNA sequencing (Retrogen Inc., San Diego, CA, USA).

For overexpression of the gp16 constructs, plasmids were transformed into *E. coli* BL21 (DE3) RIPL competent cells. The cells were induced with 0.5 mM IPTG at 30°C for 2.5-3.5 h. For gp16 purification, the induced cells were harvested by centrifugation at 8200 × *g* for 15 min at 4°C and lysed using an Aminco French press (Thermo Fisher Scientific, Inc.; buffer used: 20 mM Tris–Cl pH 8, 100 mM NaCl and 20 mM imidazole). Cell lysates were centrifuged at 34 000 × *g* for 20 min at 4°C and the supernatants containing gp16 were subjected to successive chromatography on HisTrap HP (affinity for the hexa-histidine tag) and HiLoad 16/600 Superdex 200 (size-exclusion) columns using AKTA-PRIME and AKTA-FPLC systems (GE Healthcare Bio-Sciences Corp., Piscataway, NJ, USA), respectively. HisTrap chromatography was performed using the following buffers: binding and washing—20 mM Tris–Cl pH 8, 100 mM NaCl, and 20 mM imidazole; elution–linear gradient of 20–400 mM imidazole in 20 mM Tris–Cl pH 8.0 and 100 mM NaCl. The peak gp16 fractions were loaded on to the Superdex 200 column and the size exclusion chromatography was performed in a buffer containing 20 mM Tris–HCl, pH 8 and 100 mM NaCl. The peak fractions were concentrated using Amicon Ultra15 filters (10 kDa molecular weight cut-off, Millipore, Merck KGaA, Darmstadt, Germany) and stored at −80°C in the same buffer. These proteins were used in the experiments described in 'Results' section.

Structural modeling of gp16 oligomerization domain

The 12-mer structural model of phage T4 gp16 was generated by using the X-ray structure of the 12-mer gp16 oligomerization domain from the T4-related phage 44RR (PDB code 3TXS) which shows 86% sequence similarity (69% sequence identity) to the T4 domain (25). Initial models were generated using the SWISS-MODEL automatic comparative protein modeling server (42,43). The pairwise sequence alignment of TerS domains from T4 and 44RR was done using the ClustalW alignment protocol (44) and the result was submitted to the alignment interface of SWISS-MODEL. Energy minimization of the model was then performed by PHENIX (45). The model is fully consistent with the mutational analyses performed in previous studies (39).

Analysis of *in vivo*-bound gp16-DNA complex

The gp16 expressed in *E. coli* binds to the DNA present in the cell and purifies as gp16-DNA complex. The gp16 proteins purified as above were electrophoresed on a 4–20% gradient native polyacrylamide gel (Life Technologies, Thermo Fisher Scientific, Inc.) under non-denaturing conditions using 1× Tris/borate/EDTA buffer (89 mM Tris–HCl, pH 7.6, 89 mM boric acid, and 2 mM EDTA). The gel was stained with SYBR Green I (Life Technologies, Thermo Fisher Scientific, Inc.) for DNA and then with Coomassie blue R-250 for protein.

Analysis of gp16 binding to DNA *in vitro*

The gp16 proteins (20–75 μM) purified as above were mixed with the 500-bp PCR amplified *g16* DNA (5 nM) in a buffer containing 15 mM Tris–HCl, pH 8 and 75 mM NaCl) and incubated at room temperature for 15 min. The reaction mixture was electrophoresed on a 4–20% gradient polyacrylamide gel in 1× Tris/borate/EDTA buffer (89 mM Tris, pH 7.6, 89 mM boric acid and 2 mM EDTA). The gel was first stained for DNA with SYBR Green I and then for protein with Coomassie blue R-250.

Marker rescue

Escherichia coli BL21 (DE3) RIPL (*sup*$^-$) cells containing the gp16 mutant plasmid constructs were mixed with *g16*Q114am phage and incubated at 37°C for 7 min. The infection mixtures were spotted on a lawn of *E. coli* P301 and the plates were incubated at 37°C overnight. This enabled recombinational exchange of the *g16* mutant sequences into T4 genome. The plasmids of WT and functional *g16* sequences were able to rescue the amber mutant and formed plaques and lysed the *E. coli* present in the spot. Those carrying non-functional *g16* mutant sequences were unable to form plaques (40).

Transfer of gp16 mutations into phage T4 genome

The *E. coli* BL21 (DE3) RIPL cells (*sup*$^-$) carrying the gp16 mutant recombinant plasmids were infected with *g16*Q114am mutant phage at a multiplicity of infection (MOI) of 4 and the infected cultures were incubated at 37°C for 1 h. The *E. coli* cells were lysed by addition of a few drops of chloroform to release the progeny phage. The phage were titered on *E. coli* P301 (*sup*$^-$) and individual plaques were recovered and plaque-purified. Single plaques were used for amplification of *g16* and the PCR products were sequenced to confirm incorporation of the respective mutation into the T4 genome. Single plaques for each of the mutants were used to make phage stocks on *E. coli* P301.

Phage yield of the gp16 mutants

The average yield of progeny phage produced by each gp16 mutant phage was determined by infecting *E. coli* P301 with the mutant phage at an MOI of 1 and lysing the cells with chloroform after 30 min at 37°C. The WT T4 phage was used as a control in the same experiment. The cell debris was removed by centrifugation at 8200 × *g* for 15 min at 4°C and the supernatant was titered on *E. coli* P301. The average phage yield per *E. coli* cell was calculated by dividing the total number of phage produced by the number of *E. coli* cells at the time of infection.

RESULTS

Analysis of *in vivo*-bound gp16-DNA complex

When T4 gp16 was expressed in *E. coli* from recombinant clones, it was bound to cellular DNA and purified as a protein–DNA complex. This was demonstrated by native polyacrylamide gel electrophoresis (PAGE), which showed that the Coomassie blue-stained gp16 protein bands also stained with the DNA stain SYBR Green I (Figure 3A and B, lane 1). Control proteins or certain gp16 mutant proteins that lost the ability to bind DNA were not stained with SYBR Green (see below, and data not shown). Also consistent with these results is the observation that gp16 eluted as a broad peak the shoulder of which overlapped with the void volume, suggesting the presence of high molecular weight gp16 oligomer–DNA complexes (39). The gp16-DNA interaction is strong as most of the bound DNA was resistant to pancreatic DNAse I or Benzonase (Benzonase results are shown in Figure 3C and D, lanes 2–4); only the smear (Figure 3D, lane 2), presumably the loosely bound DNA was degraded by the nucleases, while the DNA associated with the protein band showed no significant loss (Figure 3D, lane 3). The gp16 proteins from other T4-related phages such as RB69, RB49, KVP40 and 44RRR also showed similar behaviour, purifying as protein–DNA complexes (Figure 3A and B, lanes 2–5). However, the ratio of DNA to protein varied. The KVP40 and 44RR gp16s showed lower amount of bound DNA, while the RB49 gp16 showed the highest amount (Figure 3B, lane 3). Some of the latter complex dissociated during electrophoresis (see arrow). To determine the size of the DNA protected by gp16, the T4 and RB49 gp16s were treated with Benzonase to digest the loosely bound DNA followed by Proteinase K (Figure 3D, lanes 4 and 7). The size of the protected DNA was about 200-bp in the case of T4 gp16 (Figure 3D, lane 4; see arrow), and 40–60 bp in the case of RB49 gp16 (Figure 3D, lane 7; see arrows; similar results were obtained with DNAse I; data not shown). That this protected nucleic acid was indeed DNA was further confirmed by its sensitivity to DNAse I but not to RNAse A. In another control experiment, removal of the hexa-Histidine tag of gp16 by thrombin cleavage did not affect the gp16-bound DNA, demonstrating that the hexa-Histidine tag is not involved in DNA binding (data not shown).

gp16 binds DNA *in vitro*

The ability of gp16 to bind DNA *in vitro* was tested by incubating the purified gp16 with a 500-bp *g16* DNA fragment and analyzing the reaction mixture by Native-PAGE (Figure 4). As described above, the purified gp16 contained the *in vivo*-bound DNA as it could not be removed by Benzonase treatment. The size of the 500-bp DNA band shifted as evidenced by the appearance of a slow-migrating band (and a few minor ones) in the presence of gp16 and the intensity of this major band increased significantly with increasing amount of gp16 (Figure 4B, lanes 2–4; position marked with a dotted line; note that this band is absent in the control lane 5). However, there was no visible protein stain associated with this band (Figure 4A, lanes 2–4) suggesting that only a small amount of gp16 that is unoccupied by *in vivo*-bound DNA is available to participate in DNA binding. This is consistent with the above data showing that most of the purified gp16 was already associated with DNA bound *in vivo*, which, as expected, stained positive for both protein and DNA (Figure 4, higher molecular weight bands in lanes 2–5). Similar results were obtained when DNA fragments from other parts of the T4 genome were used in the binding experiments suggesting the lack of sequence specificity (data not shown).

The central channel of gp16 TerS contains potential DNA binding residues

The 11-mer and 12-mer structures of gp16 from T4-related phage 44RR and the homology models of T4 gp16 show a 40Å-long channel formed by two long anti-parallel helices (α1 and α2) connected by a sharp turn (Figure 5A and B) (25). These helices show 86% sequence similarity (69% identity) and have been extensively characterized in the case of T4 gp16 by mutational analyses (39). The functional data are fully consistent with the inter-helical interactions determined by X-ray structures of 44RR or the gp16 model. Furthermore, no significant differences in the inter-helical interactions or orientation of the channel residues were observed between the 11-mer and 12-mer structures (r.m.s.d. of 0.43Å (25)). The α2 helices line the inner surface of the channel whereas the α1 helices form the outer layer of the barrel. The 11-mer channel has an inner diameter of 32 Å at the wider end and 23 Å at the narrower end, whereas the 12-mer has an inner diameter of 38 Å at the wider end and 27 Å at the narrower end. Thus, the channel, whether formed by an 11-mer or 12-mer gp16 oligomer, can accommodate the 23 Å diameter dsDNA.

The helix α2 consists of four positively charged residues; R98, K102, K105 and K108. Of these, the K105 residue forms electrostatic interactions with the residues D106 and D109 of the helix α2 of the neighboring subunit. These are part of the two heptad repeats, a signature characteristic of coiled-coils (heptad-1 amino acids 100–106 includes K105 and D106 and heptad-2 amino acids 107–113 includes D109; Figure 5C and D) (39). K105 is therefore involved the coiled-coil interactions and hence unlikely to participate in DNA binding. However, the side chains of R98, K102 and K108 are projected into the central channel and could make contacts with the phosphate backbone of dsDNA (Figure 5C).

The positively charged residues in gp16 channel are not essential for DNA binding

DNA threading models predict that the residues in the channel, in particular the four positively charged residues, bind the DNA during the ratcheting process. To test if these residues are involved in DNA binding, we constructed two mutants, 3M and 4M. In the mutant 3M, the residues R98, K102 and K108 of helix α2 were substituted with alanine (Figure 6A). In the mutant 4M, the fourth positively charged residue, K105, was also mutated to alanine. Size-exclusion chromatography profiles showed that both mutants, similar to the WT gp16, produced high molecular weight oligomers that eluted immediately after the void volume (Figure 6B, peaks a). However, not unexpectedly, the

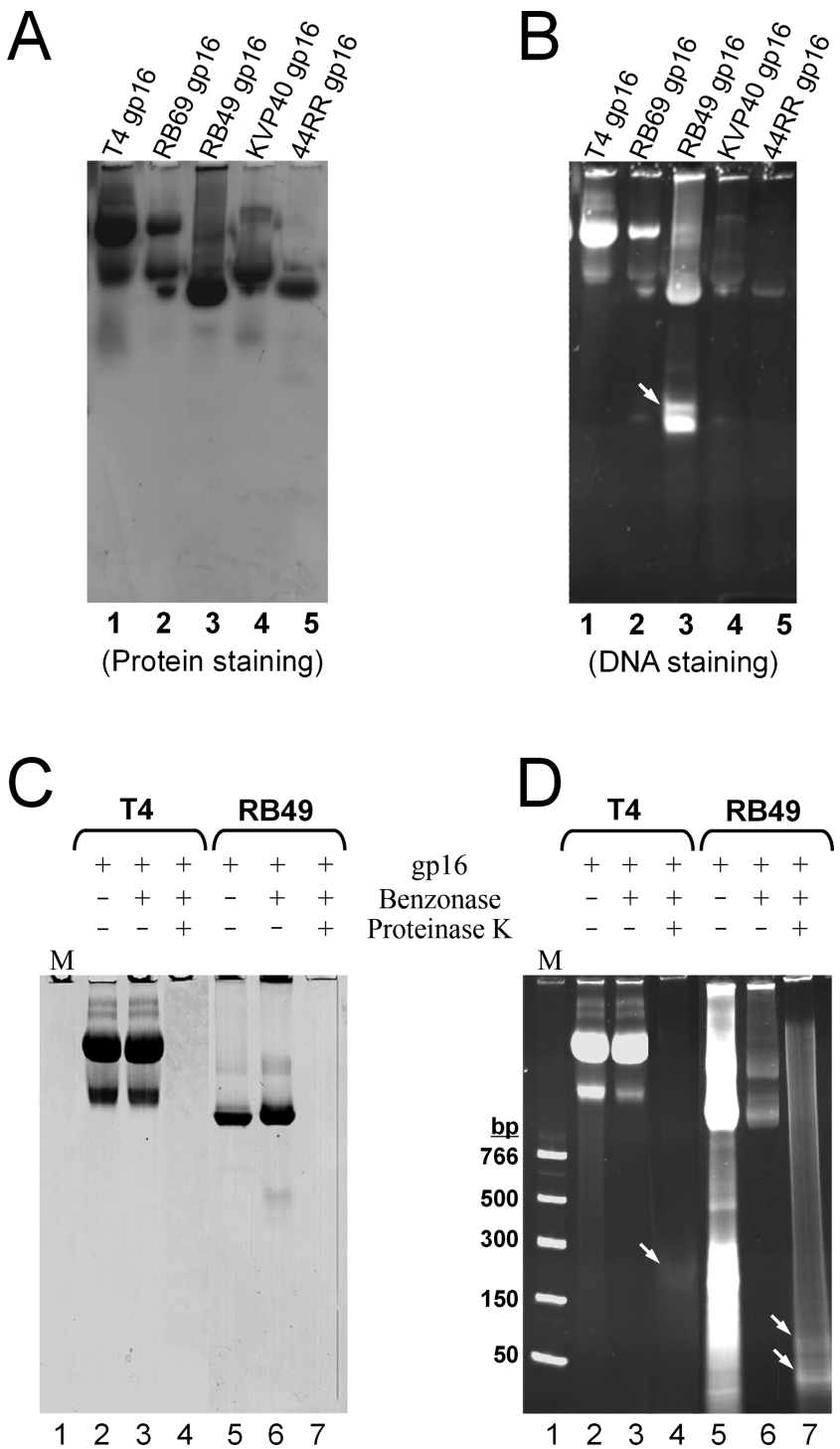

Figure 3. Analysis of *in vivo*-bound gp16-DNA complex. (A and B) Purified gp16 from phage T4 and related phages (8 μg each) were electrophoresed on a native 4–20% gradient polyacrylamide gel. The same gel was stained with Coomassie blue for protein (**A**) and SYBR Green I for DNA (**B**). The arrow corresponds to a fragment of DNA that was dissociated from RB49 gp16 during electrophoresis (panel B, lane 3). (C and D) Most of the gp16-bound DNA is resistant to Benzonase. The purified T4 and RB49 gp16 proteins (1 mg) were treated with Benzonase (Novagen) overnight at room temperature to digest the loosely-bound DNA fragments. Benzonase was removed by passing the samples through a HiLoad 16/600 Superdex 200 size-exclusion column. The tightly bound nuclease-protected DNA was then released by digesting gp16 with Proteinase K (Thermo Scientific) at 65°C for 30 min. Samples were analyzed on a 4–20% gradient polyacrylamide gel. The gel was stained with Coomassie blue for protein (**C**) and SYBR Green I for DNA (**D**). The positions of the DNA bands released from Proteinase K digestion are marked with arrows (panel D, lanes 4 and 7).

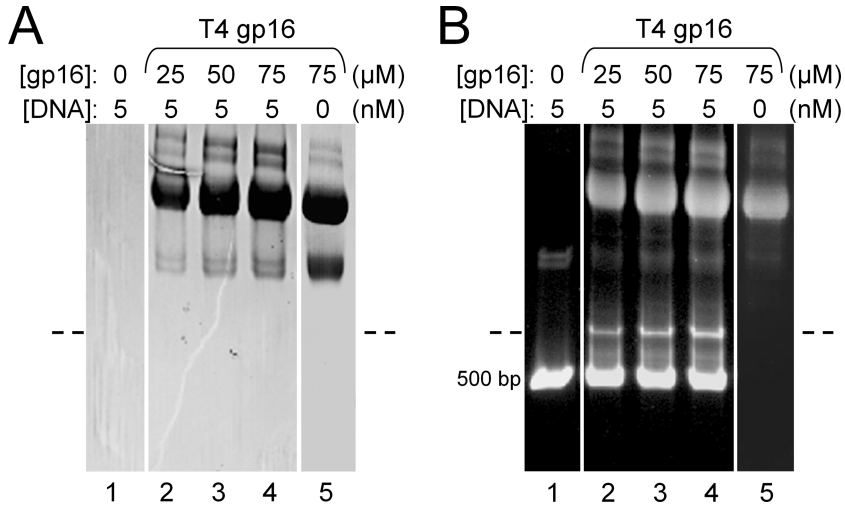

Figure 4. gp16 binds DNA *in vitro*. The purified phage T4 gp16 (25–75 μM) was incubated with the substrate DNA (500-bp amplified g16 DNA) (5 nM) in a 12 μl reaction mixture for 15 min. The reaction mixture was electrophoresed on a 4–20% gradient native polyacrylamide gel and stained with Coomassie blue for protein (**A**) and SYBR Green I for DNA (**B**). Control lanes were missing either the gp16 protein (lane 1) or the DNA (lane 5). Position of the shifted DNA band is indicated by a dashed line.

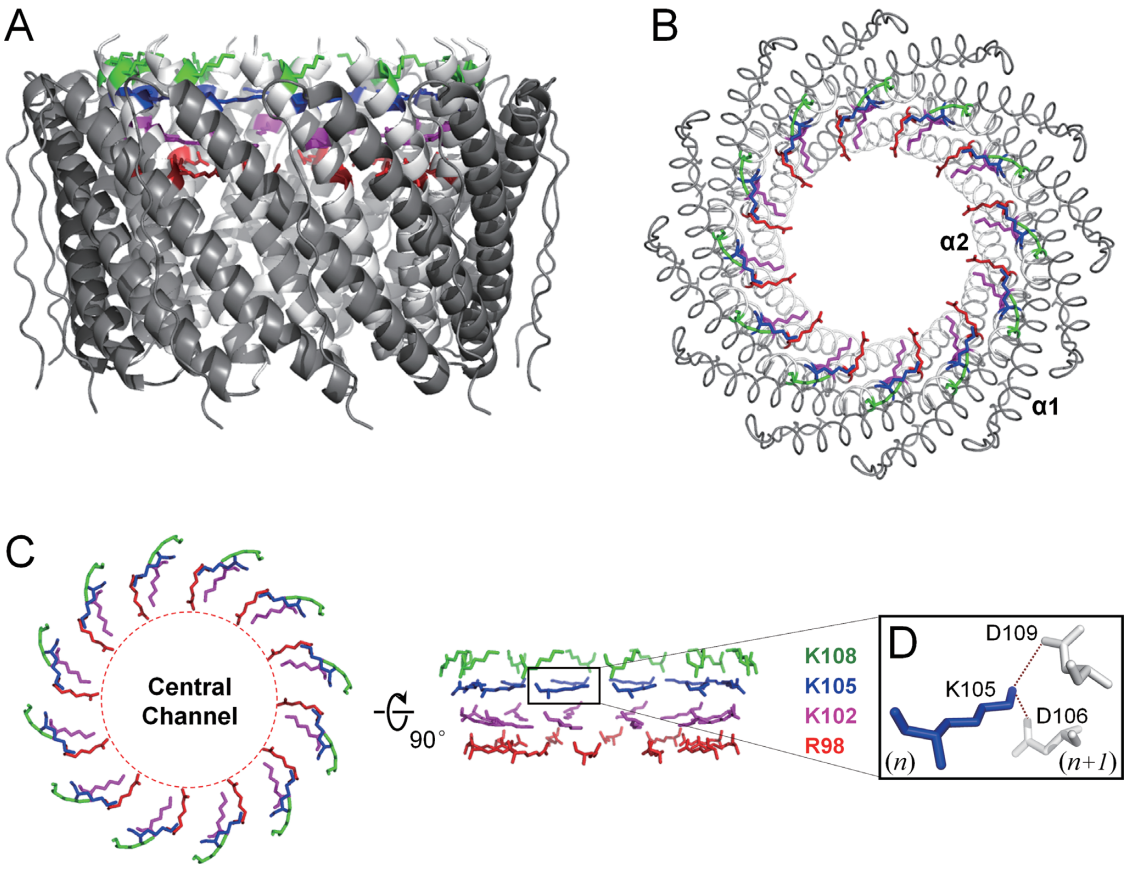

Figure 5. Potential DNA binding residues in the helix α2 of gp16's central channel. (**A** and **B**) Side- and top-views of the ribbon diagram of gp16 12-mer model showing positions of the potential DNA binding residues. The helix α2 in the lumen of the channel is shown in white and the helix α2 on the surface of the barrel is shown in gray. (**C**) Top- and side-views of the relative positions of the four potential DNA-binding residues facing the central channel (R98 in red, K102 in magenta, K105 in blue, and K108 in green). (**D**) Enlarged view showing residue K105 of the helix α2 from one subunit (*n*) interacting with the Asp residues D106 and D109 of the helix α2 from the neighboring subunit (*n* + 1).

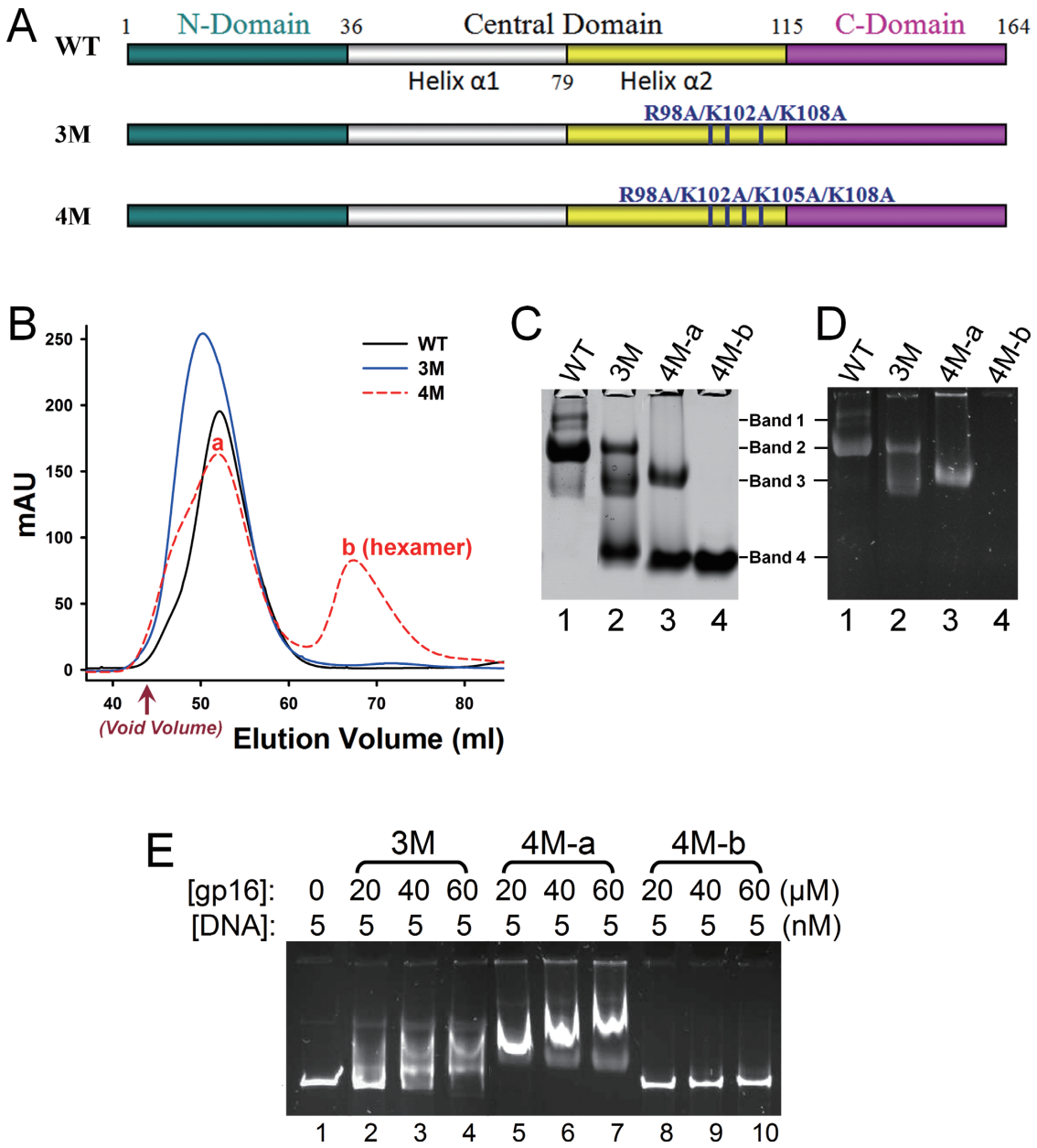

Figure 6. The positively charged residues of gp16 channel are not essential for DNA binding. (**A**) Schematic of the mutations introduced into the helix α2 of T4 gp16. Numbers represent the amino acid positions in the gp16 coding sequence. Positions of the mutated residues are indicated as black bars in helix α2. (**B**) Elution profiles of WT gp16 (black) and mutants 3M (blue) and 4M (red). The void volume is indicated by an arrow. The hexamer size of gp16 species in peak b of mutant 4M was calculated from the elution volume using the column calibrated with molecular weight standards. (C and D) The peak gp16 fractions from B were electrophoresed on a 4–20% gradient native polyacrylamide gel and stained with Coomassie blue for protein (**C**) and SYBR Green I for DNA (**D**). Lanes 4M-a and 4M-b represent the fractions from peak a and peak b of the mutant 4M. (**E**) *In vitro* DNA binding of gp16 mutants 3M and 4M. Proteins (20–60 μM) were incubated with the 500-bp g16 DNA (5 nM) in 12 μl reaction mixture for 15 min. Samples were then electrophoresed on a 4–20% gradient native polyacrylamide gel and stained with SYBR Green I. The control lane 1 contained no gp16.

4M mutant showed a second peak (peak b), approximately corresponding to a hexamer. This is consistent with the prediction that the K105A mutation would affect the coiled-coil interactions, and in turn, the oligomerization properties of gp16.

Upon native-PAGE, the WT gp16 showed one major band and a few minor bands below and above the major band (Figure 6C, lane 1; bands 1–3). We refer to these, collectively, as 'higher oligomers' (Figure 6C, peak a), which presumably contained a mixture of 11-mers, 12-mers, and multimers of these oligomers, as has been previously reported (11,28,29,39). On the other hand, the gp16 from peak b of mutant 4M showed a fast-migrating band but no higher oligomers (Figure 6C, lane 4). We refer to this and similar oligomers produced by other mutants (see below) as 'lower oligomers'. Interestingly, however, the higher oligomers of mutants 3M and 4M, unlike the WT oligomers, were unstable and dissociate into, or in equi-

librium with, the putative 'hexamers' (Figure 6C, note the presence of the fast-migrating band 4 in lanes 2 and 3, but not in lane 1; the molecular weight of this species corresponded to gp16 hexamer based on its elution volume from Superdex 200 size-exclusion column calibrated with molecular weight standards).

DNA staining showed that the higher oligomers (bands 1–3) bound DNA *in vivo* (Figure 6D, lanes 1–3), but the lower oligomer (hexamer) band showed no bound DNA (lane 4; compare the bands in panel D with the corresponding ones in panel C). *in vitro* DNA binding assays fully agreed with these results. The higher oligomers of both the mutant proteins (3M and 4M) showed mobility shift in the presence of DNA (Figure 6E, lanes 2–7), whereas the lower oligomer from peak b of mutant 4M failed to show any mobility shift (lanes 8–10).

These analyses suggest that the positively charged residues present in the channel interior are not essential for DNA binding. Further, the data uncovered a new phenomenon; that gp16 must assemble into a large oligomer in order to be able to bind to DNA, either *in vivo* or *in vitro*.

Deletion of channel helix α2 did not disrupt DNA binding

Three deletion mutants in helix α2 that lines the channel were constructed to determine if *any* of the channel residues are essential for DNA binding. These include: Del-1 in which the C-terminal half of helix α2 was deleted, Del-2 in which the deletion extended to 11 more amino acids in the C-terminal domain, and Del-3 in which the entire helix α2 was deleted (Figure 7A). In these mutants, especially the Del-3 mutant, the internal surface of the channel would be completely different if it did still assemble into an oligomer.

Size-exclusion chromatography profiles showed that all the deletion mutants produced two types of oligomers: higher oligomers (Figure 7B, peak a) and lower oligomers (Figure 7B, peak b). The sizes of the lower oligomers roughly corresponded to hexamers in Del-2, tetramers in Del-1 and trimers in Del-3. Having lost its entire helix α2, the Del-3 mutant still showed a peak at the higher oligomer position but a much larger peak at the trimer position (Figure 7B, green elution profile). Nevertheless, significant production of both types of oligomers despite large deletions in helix α2 allowed comparison of the DNA binding properties of higher and lower oligomers.

Native PAGE data (Figure 7C) were in agreement with the elution profiles of the oligomer species by size-exclusion chromatography (Figure 7B). The high molecular weight peak a fraction contained higher oligomer species (Figure 7C, lanes 1, 3 and 5). However, unlike the WT gp16, these species are more hetero-disperse, migrating as a diffused band corresponding to bands 1–3 of the WT (shown in Figure 6C). In addition, this fraction, like the mutants 3M and 4M, showed a faster-migrating lower oligomer band (black arrow in Figure 7C), which was due to dissociation of some of the higher oligomers into lower oligomers. The position of this band corresponded to the position of the lower oligomer band from peak b (Figure 7C, lanes 2, 4 and 6; compare with the same in lanes 1, 3 and 5, respectively), and of band 4 described above (Figure 6C).

Only the higher oligomer species were associated with DNA *in vivo*, as shown by a smear of DNA at the same position as the higher oligomer protein staining (Figure 7D, lanes 1, 3, and 5), while the small oligomer band showed no DNA staining (Figure 7D, lanes 2, 4, and 6). This was further confirmed by *in vitro* DNA binding studies (Figure 7E), which showed that the higher oligomers showed a shift in the mobility of the DNA (lanes 2–4, 8–10, 14–16), whereas the small oligomer fractions showed none (lanes 5–7, 11–13, 17–19). Curiously, however, the Del-2 peak b fraction showed a faint protein band at the higher oligomer position (Figure 7C, lane 4, the upper faint band; see arrow), which also stained for DNA (Figure 7D, lane 4), indicating that some of the lower oligomers might be able to re-associate into higher oligomers. This was also consistent with a slight shift observed in the DNA mobility in the *in vitro* DNA binding experiment (Figure 7E, lanes 12 and 13; see arrow). Also of note is that the Del-3 higher oligomers bound DNA better and differently from the WT higher oligomers, titrating out all the DNA into DNA–gp16 complexes most of which were retained in the well (see arrows in lanes 14–16).

The above analyses further supported the conclusions from the 3M and 4M mutant studies in that the channel helix is not essential for DNA binding whereas the size of the oligomer is.

The channel mutants produce infectious phage *in vivo*

Although the channel residues are not essential for DNA binding, they might be essential for another aspect of DNA packaging and hence critical for phage production. To test this possibility, all the channel mutations described above were transferred into phage T4 genome by recombinational rescue (46) (Figure 8A). The *sup*$^-$ *E. coli* [BL21 (DE3) RIPL] cells containing the mutant plasmids were infected with *16am* phage which has an amber mutation in helix α2 at residue Q114 (Figure 8A, step a). These were spotted on a lawn of *sup*$^-$ *E. coli* P301 (step b). If plaques appeared resulting in lysis and clearing of *E. coli* in the spot, it would mean that exchange of Q114 amber mutation with the channel mutations resulted in mutant phage that are viable. This was, indeed, the case (Figure 8B and D). Several plaques obtained from each lysed spot were purified on *sup*$^-$ *E. coli* P301 by serial dilution up to $\sim 10^5$ and the *g16* fragment from individual plaques was amplified by PCR and sequenced. Sequencing of several independent plaques confirmed that each mutant phage contained the deleted mutant sequence (step c). Surprisingly, all the channel mutants including the Del-3 mutant in which the entire helix α2 was deleted retained plaque forming ability (step d). No significant difference was observed in the plaque size (Figure 8B), nor was the yield of the mutant phages different from that of the WT phage (Figure 8C).

These data demonstrate that the channel helix is not essential for DNA packaging *in vivo*. It is remarkable that the entire helix α2 could be deleted without destroying gp16 function but it is important to note that helix α1 forms a series of coiled coil interactions with its neighbors (two hydrogen bonds, three salt bridges, and three hydrophobic interactions with each of its neighbors) (25). Furthermore, the C-terminal β-strands oligomerize to form a β-barrel

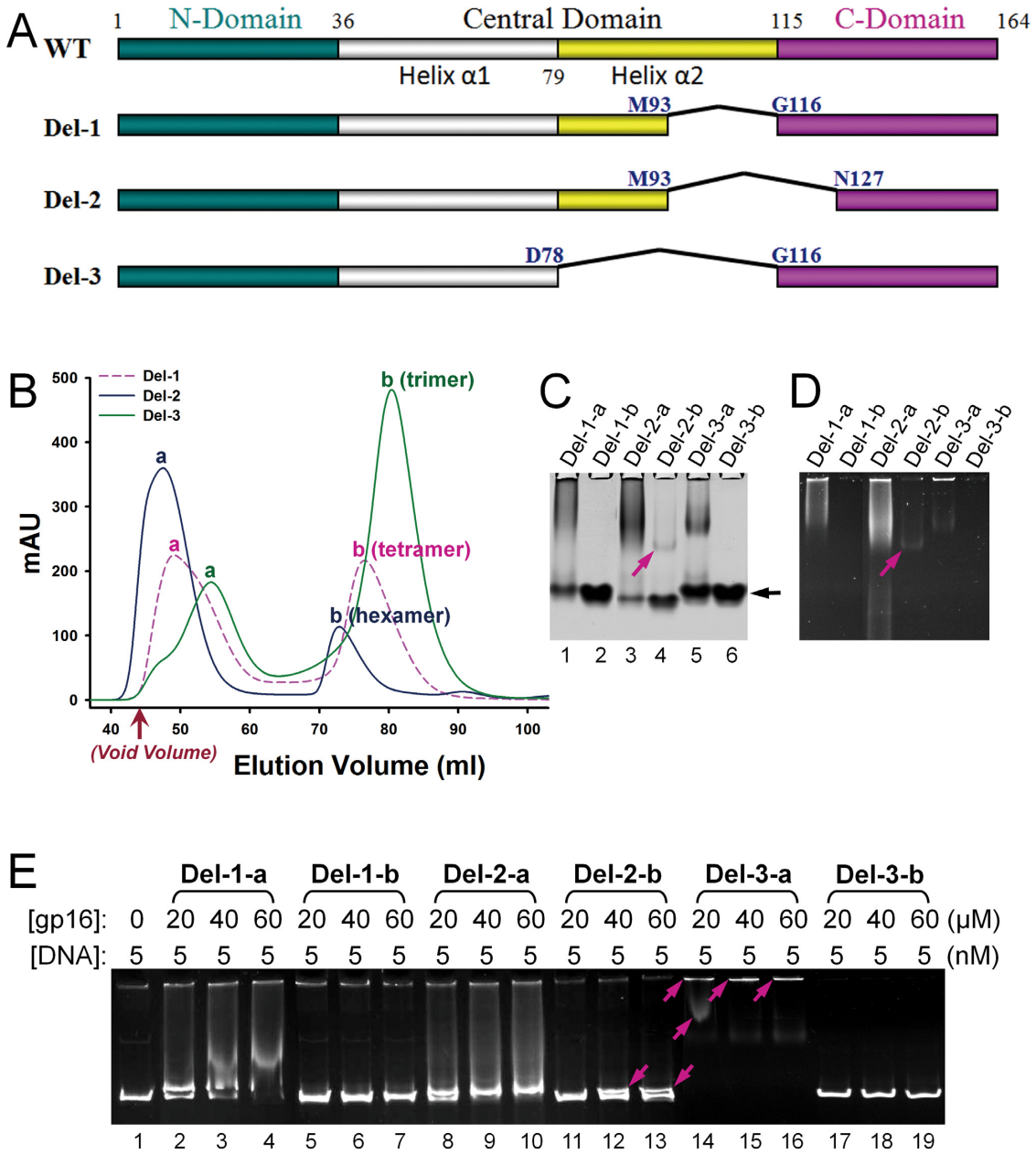

Figure 7. Deletion of channel helix α2 did not disrupt DNA binding. (**A**) Schematic of the central domain helix α2 deletion mutants. Numbers represent the amino acid positions in the gp16 coding sequence. Deleted sequences are shown by polylines and the amino acid residues flanking the deletions are shown in blue. (**B**) Elution profiles of mutants Del-1 (magenta), Del-2 (blue) and Del-3 (green). The void volume is indicated by an arrow. The oligomeric state of the gp16 species in peak b of the mutants was calculated from the elution volume. (C and D) The peak gp16 fractions from B were electrophoresed on a 4–20% gradient native polyacrylamide gel and stained with Coomassie blue for protein (**C**) and SYBR Green I for DNA (**D**). 'a' and 'b' correspond to the fractions from the peaks a and b of the respective mutant. (**E**) *In vitro* DNA binding of the deletion mutants. The purified proteins (20–60 μM) were incubated with the 500-bp g16 DNA (5 nM) in 12 μl reaction mixture for 15 min. Samples were then electrophoresed on a 4–20% gradient native polyacrylamide gel and stained with SYBR Green I. The control lane 1 contained no gp16 and shifted bands are shown by arrows in lanes 12–16.

(23,24,26). Thus, it is not entirely surprising that the helix α2 deletion mutant can still oligomerize and functional, even though its oligomer structure might be different from that of the WT (see above). It is also consistent with our other observations that suggest that a larger surface of gp16 oligomer which exposes the DNA binding N- and/or C-domains, but not the helix α2 channel, is what is important for function.

The oligomerization domain is essential for function

Next we constructed a series of additional deletions (Figure 8D), including two mutants that extend beyond helix α2 into the C-domain (amino acids deleted: 94–119; 94–123) and another mutant that lacks both helix α1 and helix α2 (amino acids deleted: 36–118) (see Figure 7A for the boundaries of helix α1 and helix α2). In the latter mutant, the N- and C-domains are fused together and also referred

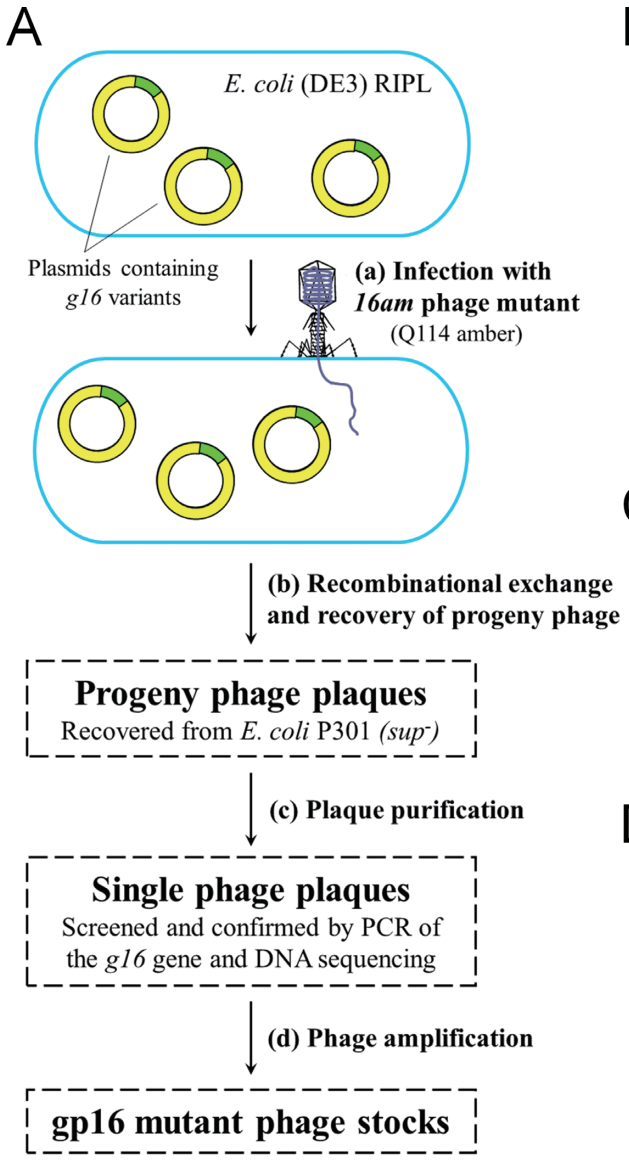

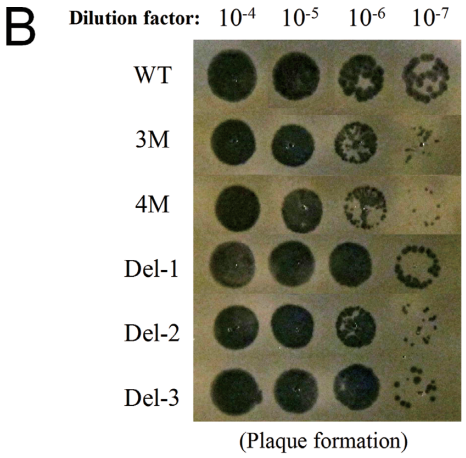

C

gp16 mutants	Phage yield/*E. coli* cell (PFU)
WT	192 ± 36
3M	105 ± 18
4M	90 ± 27
Del-1	130 ± 29
Del-2	125 ± 35
Del-3	175 ± 20
Q114 amber	0.015 ± 0.01

D

gp16 mutants	Marker Rescue
AA 81-115 deletion	+
AA 85-115 deletion	+
AA 88-115 deletion	+
AA 90-115 deletion	+
AA 94-119 deletion	+
AA 94-123 deletion	+
AA 36-118 deletion	-
Q114 amber	-

Figure 8. T4 phage mutants in the channel helix α2 produce infectious phages *in vivo*. (**A**) A flow chart showing the recombination strategy used to transfer the mutations in the central domain helix α2 into the phage T4 genome. (a) During infection, recombinational exchange occurs between the g16 mutant sequences on the plasmid and the g16Q114am mutation in the T4 genome. Infectious progeny formed plaques on *E. coli* P301 (sup-) strain (b). Individual plaques were purified by titrating on *E. coli* P301 and isolating single plaques (c). The g16 plasmids obtained from the single plaques in (c) were PCR-amplified and sequenced to confirm that the phage genome contained the expected g16 mutant sequence. The mutant plaques were grown on *E. coli* P301 to produce phage stocks (d). (**B**) The deletion gp16 helix α2 mutant phage stocks were tested for plaque forming ability on a lawn of *E. coli* P301. The WT T4 phage was used as a control. (**C**) Comparison of the average yield of the gp16 helix α2 mutant phages with the WT phage. (**D**) Marker rescue of additional gp16 helix α2 deletion mutants.

to as N-C fusion (25). These mutants were tested for plaque formation by the marker rescue assay. Consistent with the above results, none of the deletions involving helix α2 including the one that extended by eight amino acids into the C-domain affected gp16 function as they all showed positive marker rescue. However, the N-C fusion mutant that lacked the oligomerization domain showed null phenotype as it produced no plaques. This protein also lost the ability to oligomerize and produced only dimers, as determined by size-exclusion chromatography. Previous studies showed that it retained some of the functions of gp16, stimulation of gp17 ATPase and inhibition of gp17 nuclease (25). Collectively, these data showed that even though deletion of inner layer of TerS channel was tolerated, deletion of the entire oligomerization domain was not.

The oligomerization domain alone is unable to bind DNA

To determine if the oligomer ring itself is sufficient for DNA binding, we constructed a gp16 mutant consisting of only the oligomerization domain by deleting both the N- and C-terminal domains (Figure 9A). Size-exclusion chromatography profile showed that this mutant eluted as a sharp sym-

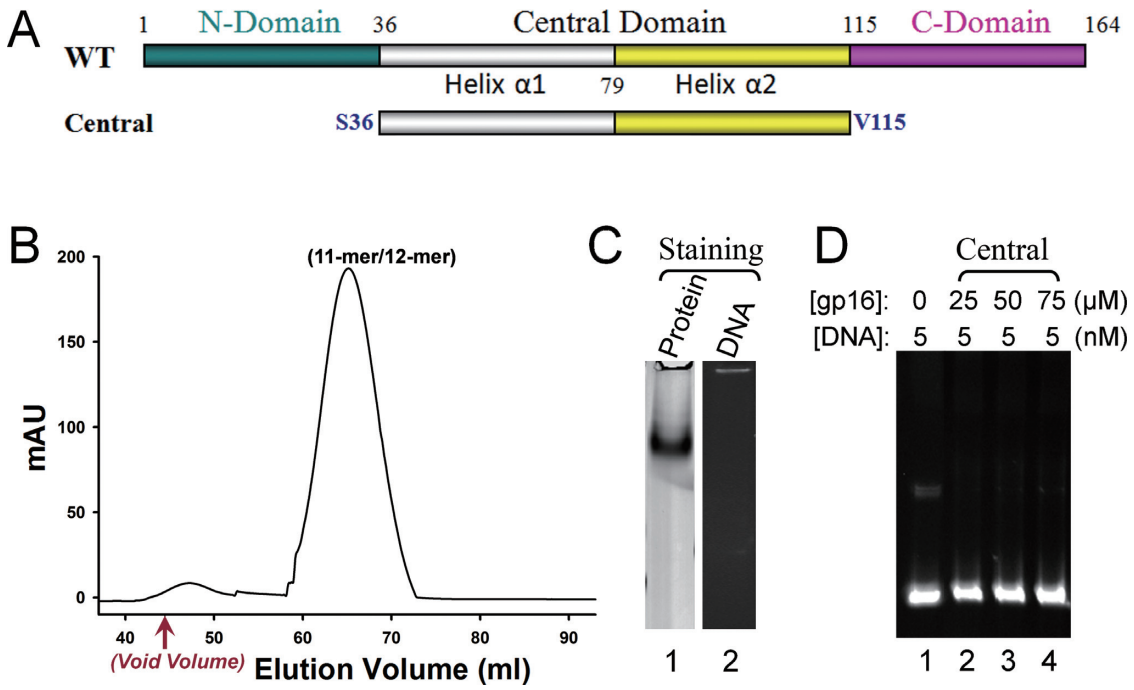

Figure 9. The oligomerization domain alone is insufficient for DNA binding. (**A**) Schematic of the oligomerization domain deletion construct. Numbers represent the amino acid positions in the gp16 coding sequence. (**B**) Elution profile of the gp16 oligomerization domain deletion mutant. The void volume is indicated by an arrow. Oligomeric state of the domain was calculated from the elution volume. (**C**) The peak fraction from (B) was electrophoresed on a 4–20% gradient native polyacrylamide gel and the gel was stained with Coomassie blue for protein (lane 1) and SYBR Green I for DNA (lane 2). (**D**) *In vitro* DNA binding of the oligomerization domain deletion mutant. The purified protein (25–75 μM) was incubated with the 500-bp g16 DNA (5 nM) in a 12 μl reaction mixture for 15 min. Samples were then electrophoresed on a 4–20% gradient native polyacrylamide gel and stained with SYBR Green I. The control lane 1 contained no gp16.

Table 1. Diameters at the narrowest points of the TerS channel from different phages

TerS from phage	Channel diameter at the narrowest Point of the central ring[a]	Channel diameter at the narrowest point of the β-barrel[a]	PDB code (reference)
44RR (11-mer)	24 Å	–	3TXQ (25)
44RR (12-mer)	28 Å	–	3TXS (25)
T4 (11-mer)	23 Å	–	(25)
T4 (12-mer)	27 Å	–	(25)
SF6	11 Å	10 Å	3ZQP (26)
Sf6	11 Å	11 Å	3HEF (24)
P22	19 Å	16 Å	3P9A (23)

[a]The diameters of the channel are determined by including all the atoms present in the respective structures.
The diameters of the channel are determined by using Pymol and including all the atoms present in the respective structures. The PDB files corresponding to the TerS structures are as follows: T4-related phage 44RR (11-mer), PDB code: 3TXQ (25); T4-related phage 44RR (12-mer), PDB code: 3TXS (25); SF6, PDB code: 3ZQP (26); Sf6, PDB code: 3HEF (24); and P22, PDB code: 3P9A (23).

metrical peak with an estimated size corresponding to 11-mers and 12-mers, similar to WT gp16 (Figure 9B; the tiny peak at the void volume contains contaminating proteins but not gp16), and also migrated as a single relatively sharp band at the higher oligomer position (Figure 9C, lane 1; compare to WT shown in Figure 6C, lane 1). But contrary to the full-length gp16, the purified oligomerization domain showed no *in vivo*-bound DNA (Figure 9C, lane 2), nor did it show any DNA mobility shift in the *in vitro* DNA binding assay (Figure 9D). These results further demonstrate that the oligomerization domain alone, which contains the intact WT channel, is insufficient to bind DNA.

DISCUSSION

Genome packaging in large DNA bacteriophages and herpes viruses occurs by translocating DNA into a pre-assembled capsid through a channel created by the packaging machine (2–5). The packaging machine consists of two stacked rings of dodecameric portal and pentameric motor aligned through their central orifices. While the exact mechanism is still being debated, it is abundantly clear that the motor protein, the large terminase (TerL; gp17 in T4), by utilizing the energy released from ATP hydrolysis ratchets DNA into the capsid (12,13,47). Forces as high as 80 pN are generated (4,16). Whether the small terminase (TerS, gp16 in T4) participates in the translocation mechanism is not known and controversial (3,24–27,37,38). It was pro-

posed that the gear-shaped TerS might allow DNA threading through the central channel for genome recognition and DNA cutting during packaging initiation and for ratcheting DNA during translocation (24,26,27,38). In these models, there will be three concentric rings in the packaging machine, TerS, TerL and portal with completely mismatched symmetries.

We tested the threading models by a combination of mutational, biochemical and genetic approaches. We first established DNA binding assays to assess the ability of gp16, the T4 TerS, to bind DNA. These experiments demonstrated that the *E. coli*-expressed gp16 binds DNA, both *in vivo* and *in vitro*. Indeed, gp16 purifies as a DNA–protein complex and elutes as a broad high molecular weight peak near the void volume of the size-exclusion column. Upon separation by gel electrophoresis, the Coomassie blue-stained protein bands also stained for DNA. About 200-bp DNA was tightly bound to gp16 and was resistant to DNAse. But it was released after degradation of gp16 by Proteinase K. On the other hand, certain mutants of gp16 or lower gp16 oligomers failed to bind DNA. These data were further corroborated by *in vitro* DNA binding assays.

We argued that if TerS participates in DNA threading, some of the residues in the lumen of TerS channel must interact with the DNA. However, our analyses of a series of mutants showed no evidence of such an interaction. For instance, mutation of several basic residues whose side chains project into the channel (mutants 3M and 4M) did not result in loss of DNA binding. In fact, their binding behaviour was similar to that of the WT TerS, both *in vivo* and *in vitro*. Most striking, progressive deletions of the inner α-helix that layers the channel lumen, including a mutant that lost the entire helix retained DNA binding. Remarkably, all these mutations, when transferred into T4 genome, produced plaques and a burst of progeny similar to that of the WT, attesting to their functionality.

Many of our gp16 mutants assembled two types of oligomers, as determined by size-exclusion chromatography and mobility by native PAGE. These include: higher oligomers that, like WT gp16, presumably contained 11-mers and 12-mers (and multimers of these), and lower oligomers that ranged from trimers to hexamers. This is not unexpected because some of the mutated residues either are involved in, or indirectly affected, the coiled coil interactions that are responsible for oligomerization (37). DNA binding data showed that, regardless of the mutant, only the higher oligomers bound to DNA, either *in vitro* or *in vivo*, but the lower oligomers did not. This means that the size of the oligomer, but not the channel *per se*, is critical for DNA binding. Furthermore, another mutant that contained only the oligomerization domain, i.e. it has intact WT TerS channel but lacked the N- and C-domains, exhibited no DNA binding at all, further confirming that the channel as such has no DNA binding activity.

Why are higher TerS oligomers competent for DNA binding? Clearly, higher oligomers expose larger surface area and contain more N- and C-domains per oligomer than the lower oligomers. There is evidence that the N-domains of phages λ (30), SPP1 (31), and Sf6 (32) TerSs and the N- and C-domains of phage P22 TerS contain a DNA binding site (37). In T4, like P22, both the N- and C-domains of gp16 are involved in DNA binding (unpublished data). Consequently, the number of interactions in TerS-DNA complex will be greater, hence more stable, in a higher oligomer than in a lower oligomer. Furthermore, if, as proposed by the wrapping model, the DNA winds around the oligomer (Figure 2), the larger surface area of higher oligomers would cause less severe bending of DNA when compared to lower oligomers, thus requiring less energy to generate TerS–DNA complex (48). There is evidence that the *cos*/*pac* sequences contain an intrinsic DNA bend and DNA bending was demonstrated in the TerS-DNA complexes of phages λ, SPP1, Sf6, and P1 (31,32,36,49). Furthermore, phage λ needs a special DNA bending protein, the *E. coli* integration host factor (IHF), for *cos* cutting (36,50). Thus, our data on differential DNA binding of higher vs lower gp16 TerS oligomers combined with the available data from other phages support the DNA wrapping models (26,32) and argue against DNA threading through TerS channel.

Other observations are also consistent with the above conclusion. As mentioned earlier, the stoichiometry of TerS oligomers varies in different phages (24–26,37), and even in the TerS produced from the same phage (25,27,37,38). If TerS is essential for DNA threading, a conserved stoichiometry would be expected in order to allow for specific interactions between the channel and the DNA. Furthermore, the diameter of Sf6, SF6, and P22 TerS channel at the narrowest point is too small to accommodate the 23 Å double-stranded DNA. Only the T4 channel with a diameter of about 23–27 Å is large enough (Table 1). Even in this case, as our data demonstrated, the channel is not essential. It can be argued, however, that the TerS stoichiometry might be different and the channel might be wider when assembled in the presence of TerL. While this cannot be ruled out, evidence suggests otherwise. In phage P22, the TerS–TerL complex is a nanomer of TerS bound to two molecules of TerL and the stoichiometry of TerS is the same whether it is assembled in the presence or absence of TerL (51). The phage λ TerS (gpNu1)-TerL (gpA) complex is a tetramer of heterotrimers, $(TerS_2{:}TerL_1)_4$ (52,53). This complex is highly active for *cos*-cutting and is reported to form a ring structure, presumably containing an octamer ring of gpNu1. Considering that gpNu1 has similar size and domain organization as the other TerSs, an octamer channel of gpNu1 would unlikely be wide enough for DNA threading.

Extensive sequence analyses by Casjens and co-workers revealed that unlike the TerL sequences that are relatively well-conserved, the TerS sequences, even among the related phages, are variable (34). Our data implicate that these variations, in addition to modifying the genome recognition site (34), alter the stoichiometry of TerS oligomer in order to optimize its outer surface for capturing the viral genome. Indeed, certain phage P22 mutants selected for high frequency transduction of host genome show a switch in TerS stoichiometry from nanomer to decamer (3,27,38), as the latter probably increased the promiscuity of genome recognition. An optimal TerS outer surface might be essential to generate a metastable TerS–DNA–TerL ternary complex that upon cleavage by TerL would be destabilized and remodelled as a translocation complex. TerL can then attach the complex to its portal partner and TerS activates

TerL's packaging ATPase to jump-start DNA translocation (23,25,54).

TerS's function has probably evolved to link the newly replicated viral genome to the packaging machinery. This must occur at high fidelity and efficiency because, otherwise, it could lead to mismatching of genomes and capsids in a host infected with more than one virus, a common occurrence in nature. The three-domain architecture of TerS allows evolutionary flexibility to optimize this process, for instance by exchanging domains, to modulate genome recognition (N-domain), stoichiometry (oligomerization domain) and/or TerL regulation (C-domain). In addition to capturing the right genome, this would allow tight regulation of packaging initiation that in some ways is reminiscent of the regulation of genome expression by nucleosome structure in higher organisms (55,56). It might also allow incorporation of novel genes from host or another virus into the capsid, thus providing survival advantages to the virus as well as aid in the horizontal evolution of the host genome (34).

ACKNOWLEDGEMENTS

The authors thank Dr Victor Padilla-Sanchez for his assistance with Figures 1 and 2, and Dr Ayca Akal-Strader for critically reviewing the manuscript and thoughtful suggestions.

FUNDING

National Science Foundation [MCB 1411989 to V.B.R.]; National Institutes of Health [2R01AI081726 to V.B.R., in part]; National Natural Science Foundation of China [31300652 to S.G., in part]; Jiangsu Provincial Natural Science Foundation of China [BK20130406 to S.G., in part]. Funding for open access charge: National Natural Science Foundation [31300652 to S.G.]; Jiangsu Provincial Natural Science Foundation of China [BK20130406 to S.G.
Conflict of interest statement. None declared.

REFERENCES

1. Hendrix,R.W., Smith,M.C., Burns,R.N., Ford,M.E. and Hatfull,G.F. (1999) Evolutionary relationships among diverse bacteriophages and prophages: all the world'sa phage. *Proc. Natl. Acad. Sci. U.S.A.*, **96**, 2192–2197.
2. Rao,V.B. and Feiss,M. (2008) The bacteriophage DNA packaging motor. *Annu. Rev. Genet.*, **42**, 647–681.
3. Casjens,S.R. (2011) The DNA-packaging nanomotor of tailed bacteriophages. *Nat. Rev. Microbiol.*, **9**, 647–657.
4. Chemla,Y.R. and Smith,D.E. (2012) Single-molecule studies of viral DNA packaging. *Adv. Exp. Med. Biol.*, **726**, 549–584.
5. Oliveira,L., Tavares,P. and Alonso,J.C. (2013) Headful DNA packaging: bacteriophage SPP1 as a model system. *Virus Res.*, **173**, 247–259.
6. Rao,V.B. and Feiss,M. (2015) Mechanisms of DNA Packaging by Large Double-Stranded DNA Viruses. *Annu. Rev. Virol.*, **2**, 351–378.
7. Black,L.W. and Rao,V.B. (2012) Structure, assembly, and DNA packaging of the bacteriophage T4 head. *Adv. Virus Res.*, **82**, 119–153.
8. Rao,V.B. and Black,L.W. (2005) *Viral Genome Packaging Machines: Genetics, Structure, and Mechanism*. Springer, pp. 40–58.
9. Ghosh-Kumar,M., Alam,T.I., Draper,B., Stack,J.D. and Rao,V.B. (2011) Regulation by interdomain communication of a headful packaging nuclease from bacteriophage T4. *Nucleic Acids Res.*, **39**, 2742–2755.
10. Rao,V.B. and Black,L.W. (1988) Cloning, overexpression and purification of the terminase proteins gp16 and gp17 of bacteriophage T4. Construction of a defined in-vitro DNA packaging system using purified terminase proteins. *J. Mol. Biol.*, **200**, 475–488.
11. Leffers,G. and Rao,V.B. (2000) Biochemical characterization of an ATPase activity associated with the large packaging subunit gp17 from bacteriophage T4. *J. Biol. Chem.*, **275**, 37127–37136.
12. Kondabagil,K.R., Zhang,Z. and Rao,V.B. (2006) The DNA translocating ATPase of bacteriophage T4 packaging motor. *J. Mol. Biol.*, **363**, 786–799.
13. Baumann,R.G. and Black,L.W. (2003) Isolation and characterization of T4 bacteriophage gp17 terminase, a large subunit multimer with enhanced ATPase activity. *J. Biol. Chem.*, **278**, 4618–4627.
14. Baumann,R.G., Mullaney,J. and Black,L.W. (2006) Portal fusion protein constraints on function in DNA packaging of bacteriophage T4. *Mol. Microbiol.*, **61**, 16–32.
15. Sun,L., Zhang,X., Gao,S., Rao,P.A., Padilla-Sanchez,V., Chen,Z., Sun,S., Xiang,Y., Subramaniam,S., Rao,V.B. *et al.* (2015) Cryo-EM structure of the bacteriophage T4 portal protein assembly at near-atomic resolution. *Nat. Commun.*, **6**, 7548.
16. Fuller,D.N., Raymer,D.M., Kottadiel,V.I., Rao,V.B. and Smith,D.E. (2007) Single phage T4 DNA packaging motors exhibit large force generation, high velocity, and dynamic variability. *Proc. Natl. Acad. Sci. U.S.A.*, **104**, 16868–16873.
17. Simpson,A.A., Tao,Y., Leiman,P.G., Badasso,M.O., He,Y., Jardine,P.J., Olson,N.H., Morais,M.C., Grimes,S., Anderson,D.L. *et al.* (2000) Structure of the bacteriophage phi29 DNA packaging motor. *Nature*, **408**, 745–750.
18. Lebedev,A.A., Krause,M.H., Isidro,A.L., Vagin,A.A., Orlova,E.V., Turner,J., Dodson,E.J., Tavares,P. and Antson,A.A. (2007) Structural framework for DNA translocation via the viral portal protein. *EMBO J.*, **26**, 1984–1994.
19. Padilla-Sanchez,V., Gao,S., Kim,H.R., Kihara,D., Sun,L., Rossmann,M.G. and Rao,V.B. (2014) Structure-function analysis of the DNA translocating portal of the bacteriophage T4 packaging machine. *J. Mol. Biol.*, **426**, 1019–1038.
20. Olia,A.S., Prevelige,P.E. Jr, Johnson,J.E. and Cingolani,G. (2011) Three-dimensional structure of a viral genome-delivery portal vertex. *Nat. Struct. Mol. Biol.*, **18**, 597–603.
21. Zhao,H., Christensen,T.E., Kamau,Y.N. and Tang,L. (2013) Structures of the phage Sf6 large terminase provide new insights into DNA translocation and cleavage. *Proc. Natl. Acad. Sci. U.S.A.*, **110**, 8075–8080.
22. Sun,S., Kondabagil,K., Draper,B., Alam,T.I., Bowman,V.D., Zhang,Z., Hegde,S., Fokine,A., Rossmann,M.G. and Rao,V.B. (2008) The structure of the phage T4 DNA packaging motor suggests a mechanism dependent on electrostatic forces. *Cell*, **135**, 1251–1262.
23. Roy,A., Bhardwaj,A., Datta,P., Lander,G.C. and Cingolani,G. (2012) Small terminase couples viral DNA binding to genome-packaging ATPase activity. *Structure*, **20**, 1403–1413.
24. Zhao,H., Finch,C.J., Sequeira,R.D., Johnson,B.A., Johnson,J.E., Casjens,S.R. and Tang,L. (2010) Crystal structure of the DNA-recognition component of the bacterial virus Sf6 genome-packaging machine. *Proc. Natl. Acad. Sci. U.S.A.*, **107**, 1971–1976.
25. Sun,S., Gao,S., Kondabagil,K., Xiang,Y., Rossmann,M.G. and Rao,V.B. (2012) Structure and function of the small terminase component of the DNA packaging machine in T4-like bacteriophages. *Proc. Natl. Acad. Sci. U.S.A.*, **109**, 817–822.
26. Buttner,C.R., Chechik,M., Ortiz-Lombardia,M., Smits,C., Ebong,I.O., Chechik,V., Jeschke,G., Dykeman,E., Benini,S., Robinson,C.V. *et al.* (2012) Structural basis for DNA recognition and loading into a viral packaging motor. *Proc. Natl. Acad. Sci. U.S.A.*, **109**, 811–816.
27. Nemecek,D., Lander,G.C., Johnson,J.E., Casjens,S.R. and Thomas,G.J. Jr (2008) Assembly architecture and DNA binding of the bacteriophage P22 terminase small subunit. *J. Mol. Biol.*, **383**, 494–501.
28. van Duijn,E. (2010) Current limitations in native mass spectrometry based structural biology. *J. Am. Soc. Mass Spectrom.*, **21**, 971–978.
29. Lin,H., Simon,M.N. and Black,L.W. (1997) Purification and characterization of the small subunit of phage T4 terminase, gp16, required for DNA packaging. *J. Biol. Chem.*, **272**, 3495–3501.

30. de Beer,T., Fang,J., Ortega,M., Yang,Q., Maes,L., Duffy,C., Berton,N., Sippy,J., Overduin,M., Feiss,M. *et al.* (2002) Insights into specific DNA recognition during the assembly of a viral genome packaging machine. *Mol. Cell*, **9**, 981–991.
31. Chai,S., Lurz,R. and Alonso,J.C. (1995) The small subunit of the terminase enzyme of Bacillus subtilis bacteriophage SPP1 forms a specialized nucleoprotein complex with the packaging initiation region. *J. Mol. Biol.*, **252**, 386–398.
32. Zhao,H., Kamau,Y.N., Christensen,T.E. and Tang,L. (2012) Structural and functional studies of the phage Sf6 terminase small subunit reveal a DNA-spooling device facilitated by structural plasticity. *J. Mol. Biol.*, **423**, 413–426.
33. Gao,S. and Rao,V.B. (2011) Specificity of interactions among the DNA-packaging machine components of T4-related bacteriophages. *J. Biol. Chem.*, **286**, 3944–3956.
34. Leavitt,J.C., Gilcrease,E.B., Wilson,K. and Casjens,S.R. (2013) Function and horizontal transfer of the small terminase subunit of the tailed bacteriophage Sf6 DNA packaging nanomotor. *Virology*, **440**, 117–133.
35. Frackman,S., Siegele,D.A. and Feiss,M. (1984) A functional domain of bacteriophage lambda terminase for prohead binding. *J. Mol. Biol.*, **180**, 283–300.
36. Catalano,C.E., Cue,D. and Feiss,M. (1995) Virus DNA packaging: the strategy used by phage lambda. *Mol. Microbiol.*, **16**, 1075–1086.
37. Bhardwaj,A., Casjens,S.R. and Cingolani,G. (2014) Exploring the atomic structure and conformational flexibility of a 320 A long engineered viral fiber using X-ray crystallography. *Acta Crystallogr. D Biol. Crystallogr.*, **70**, 342–353.
38. Nemecek,D., Gilcrease,E.B., Kang,S., Prevelige,P.E. Jr, Casjens,S. and Thomas,G.J. Jr (2007) Subunit conformations and assembly states of a DNA-translocating motor: the terminase of bacteriophage P22. *J. Mol. Biol.*, **374**, 817–836.
39. Kondabagil,K.R. and Rao,V.B. (2006) A critical coiled coil motif in the small terminase, gp16, from bacteriophage T4: insights into DNA packaging initiation and assembly of packaging motor. *J. Mol. Biol.*, **358**, 67–82.
40. Rao,V.B. and Mitchell,M.S. (2001) The N-terminal ATPase site in the large terminase protein gp17 is critically required for DNA packaging in bacteriophage T4. *J. Mol. Biol.*, **314**, 401–411.
41. Horton,R.M., Hunt,H.D., Ho,S.N., Pullen,J.K. and Pease,L.R. (1989) Engineering hybrid genes without the use of restriction enzymes: gene splicing by overlap extension. *Gene*, **77**, 61–68.
42. Biasini,M., Bienert,S., Waterhouse,A., Arnold,K., Studer,G., Schmidt,T., Kiefer,F., Cassarino,T.G., Bertoni,M. and Bordoli,L. (2014) SWISS-MODEL: modelling protein tertiary and quaternary structure using evolutionary information. *Nucleic Acids Res.*, **42**, W252–W258.
43. Arnold,K., Bordoli,L., Kopp,J. and Schwede,T. (2006) The SWISS-MODEL workspace: a web-based environment for protein structure homology modelling. *Bioinformatics*, **22**, 195–201.
44. Goujon,M., McWilliam,H., Li,W., Valentin,F., Squizzato,S., Paern,J. and Lopez,R. (2010) A new bioinformatics analysis tools framework at EMBL–EBI. *Nucleic Acids Res.*, **38**, W695–W699.
45. Adams,P.D., Afonine,P.V., Bunkóczi,G., Chen,V.B., Davis,I.W., Echols,N., Headd,J.J., Hung,L.-W., Kapral,G.J. and Grosse-Kunstleve,R.W. (2010) PHENIX: a comprehensive Python-based system for macromolecular structure solution. *Acta Crystallogra. D: Biol. Crystallogr.*, **66**, 213–221.
46. Mitchell,M.S. and Rao,V.B. (2004) Novel and deviant Walker A ATP-binding motifs in bacteriophage large terminase-DNA packaging proteins. *Virology*, **321**, 217–221.
47. Dhar,A. and Feiss,M. (2005) Bacteriophage lambda terminase: alterations of the high-affinity ATPase affect viral DNA packaging. *J. Mol. Biol.*, **347**, 71–80.
48. Vologodskii,A. and Frank-Kamenetskii,M.D. (2013) Strong bending of the DNA double helix. *Nucleic Acids Res.*, **41**, 6785–6792.
49. Sternberg,N. and Coulby,J.N. (1988) Processing of the bacteriophage P1 packaging site (pac) is regulated by adenine methylation. *Gene*, **74**, 203.
50. Xin,W., Cai,Z.H. and Feiss,M. (1993) Function of IHF in lambda DNA packaging. II. Effects of mutations altering the IHF binding site and the intrinsic bend in cosB on lambda development. *J. Mol. Biol.*, **230**, 505–515.
51. McNulty,R., Lokareddy,R.K., Roy,A., Yang,Y., Lander,G.C., Heck,A.J., Johnson,J.E. and Cingolani,G. (2015) Architecture of the complex formed by large and small terminase subunits from bacteriophage P22. *J. Mol. Biol.*, **427**, 3285–3299.
52. Maluf,N.K., Gaussier,H., Bogner,E., Feiss,M. and Catalano,C.E. (2006) Assembly of bacteriophage lambda terminase into a viral DNA maturation and packaging machine. *Biochemistry*, **45**, 15259–15268.
53. Andrews,B.T. and Catalano,C.E. (2013) Strong subunit coordination drives a powerful viral DNA packaging motor. *Proc. Natl. Acad. Sci. U.S.A.*, **110**, 5909–5914.
54. Vafabakhsh,R., Kondabagil,K., Earnest,T., Lee,K.S., Zhang,Z., Dai,L., Dahmen,K.A., Rao,V.B. and Ha,T. (2014) Single-molecule packaging initiation in real time by a viral DNA packaging machine from bacteriophage T4. *Proc. Natl. Acad. Sci. U.S.A.*, **111**, 15096–15101.
55. Zhu,P. and Li,G. (2016) Structural insights of nucleosome and the 30-nm chromatin fiber. *Curr. Opin. Struct. Biol.*, **36**, 106–115.
56. Cutter,A.R. and Hayes,J.J. (2015) A brief review of nucleosome structure. *FEBS Lett.*, **589**, 2914–2922.